Supplementary Information for ***Dalton Transactions***

Ag-based coordination polymer-enhanced photocatalytic degradation of ciprofloxacin and p-nitrophenol

Zhihu Ma,[a] Xiaoming Song,[a] Zhaoyu Li,[a] Yixia Ren,[*a] Jijiang Wang[a] and Yucang Liang[*b]

[a] Laboratory of New Energy and New Function Materials, Shaanxi Key Laboratory of Chemical Reaction Engineering, College of Chemistry and Chemical Engineering, Yan'an University, Yan'an 716000, China
Email: renyx@yau.edu.cn

[b] Institut für Anorganische Chemie, Eberhard Karls Universität Tübingen, Auf der Morgenstelle 18, 72076 Tübingen, Germany
Email: yucang.liang@uni-tuebingen.de

Section I

Materials and instruments

$AgNO_3$ (AR analytical purity) from China Pharmaceutical Group Shanghai Chemical Reagent Company, tri-(4-imidazole phenyl) amine (TIPA) from Jinan Hengchem Ni., Ltd, ethanol, N-N dimethylacetamide (DMA), ethanol (C_2H_5OH, AR), N, and N-dimethylformamide (DMF) from Tianjin Comio Chemical Reagent Co. Ltd., p-nitrophenol (BPA), and ciprofloxacin (CIP) from Shanghai Maclean Biochemical Technology Co., *tert*-butanol, ammonium oxalate, and p-benzoquinone (BQ, 99%) from Sinopharm Holding Chemical Reagent Co., were purchased and used without further purification. Deionized water was generated by UPP ultrapure water machine (18.25 MΩ cm^{-l} resistivity, 25 °C).

XPS equipment model from Thermo Scientific (USA) was used to calibrate all binding energy values against the C 1s peak at 284.8 eV. The crystal parameters were verified using a Bruker D2 Phase powder X-ray diffractometer (XRD) from Germany. The thermosgravimetric analysis was measured on a Hitachi 7200 (Japan). Fluorescence lifetimes were determined by FLS920 steady-state, transient fluorescence spectrometer at room temperature. UV-vis absorption and diffuse reflectance spectra were collected using UV-2550 and UV-2600 220V, CH spectrophotometers, and photocatalytic experiments were performed with XP A-7 in a photochemical reactor from XuJiang, and liquid chromatography-mass spectrometry(LC-MS) coupling using Thermo Fisher Ultimate 3000 UHPLC -Q Exactive was applied to analyze sample compositions. Inductively coupled plasma-optical emission spectroscopy (ICP-OES) was tested using an Agilent 5110 ICP-OES instrument. The samples were centrifuged using a T20 centrifuge. Transient photocurrent electrochemical impedance spectroscopy (EIS) was measured on the CHI660E electrochemical station. Photoluminescence (PL) spectra and fluorescence lifetimes were measured using an F-7100 fluorescence spectrophotometer and an FLS920 steady-state, respectively. Steady-state photoluminescence (PL) spectra, time-resolved PL decay curves, and lifetimes of photogenerated electrons were detected. The excitation

wavelength of all luminescence measurements was 482 nm, and the filter was 420 nm. The Chennai CHI600E electrochemical workstation was used to measure the electrochemical impedance spectra (EIS) and photocurrent signals. The Ag/AgCl electrode was used as the reference electrode, and the platinum wire as the counter electrode. The working electrode was prepared by coating photocatalyst onto indium tin oxide (ITO), and 0.5 M Na_2SO_4 aqueous solution was chosen as the electrolyte. The bias potential was controlled at -0.5 V. A xenon lamp light source (> 420 nm) was used as the visible light source. 5 mg of catalyst particles were added to 1 mL of ethanol and 1 mL of water solution under sonication for 2 h. The coated films were obtained at 2 × 2 cm by pipetting 2 mL of the mixture onto the ITO glass surface in portions.

Crystal structure determination

Single crystal X-ray diffraction analysis of Ag-TIPA was performed on a Bruker SMART APEX CCD diffractometer equipped with graphite monochromatic Mo Ka radiation (λ = 0.71073 Å). All data were integrated with SAINT and corrected for multiple scan absorption using SADABs. The structure was solved using the direct method of SHELXT and refined by SHELXL-2018 for F^2 by full matrix least squares. All non-hydrogen atoms were anisotropically refined. The hydrogen atoms were set at the calculated positions, and the crystal structures were plotted using Diamond 3.1 software. The crystallographic data of Ag-TIPA are provided in Table S1, and the selected bond lengths and angles are shown in Table S2.

Section II

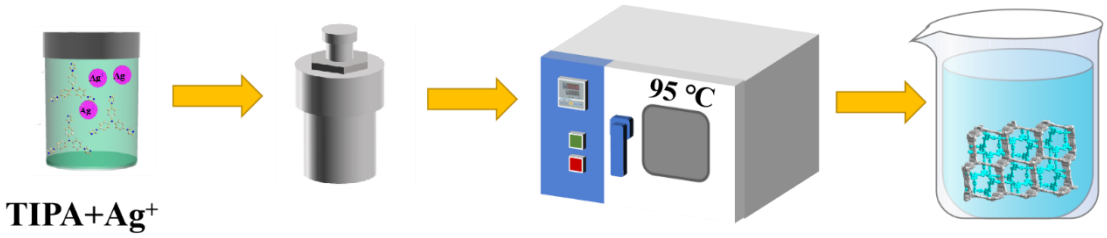

Scheme S1. The preparation of Ag-TIPA.

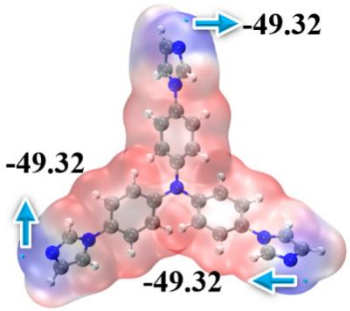

Fig. S1 The electrostatic potential of TIPA.

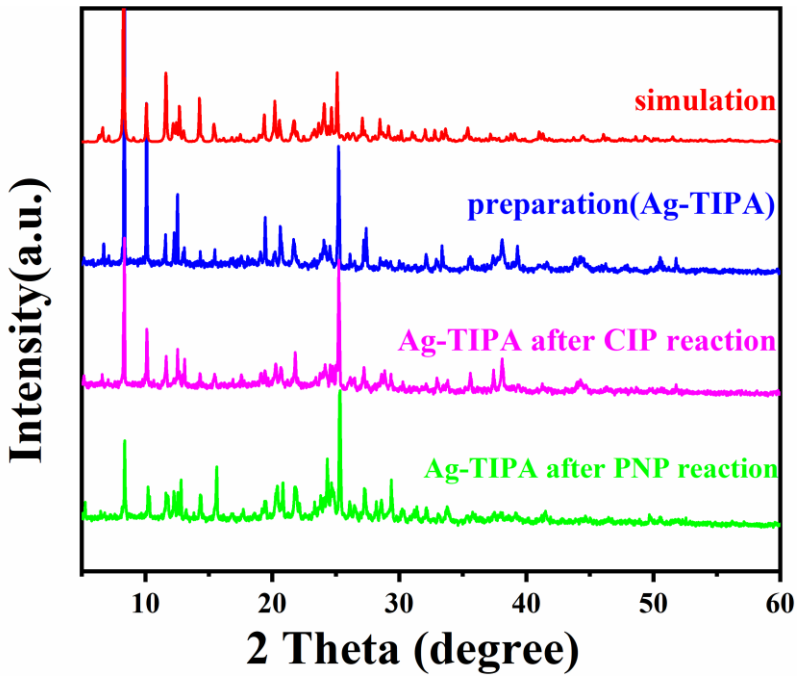

Fig. S2 A comparison of PXRD patterns between Ag-TIPA before and after catalysis and simulation curve.

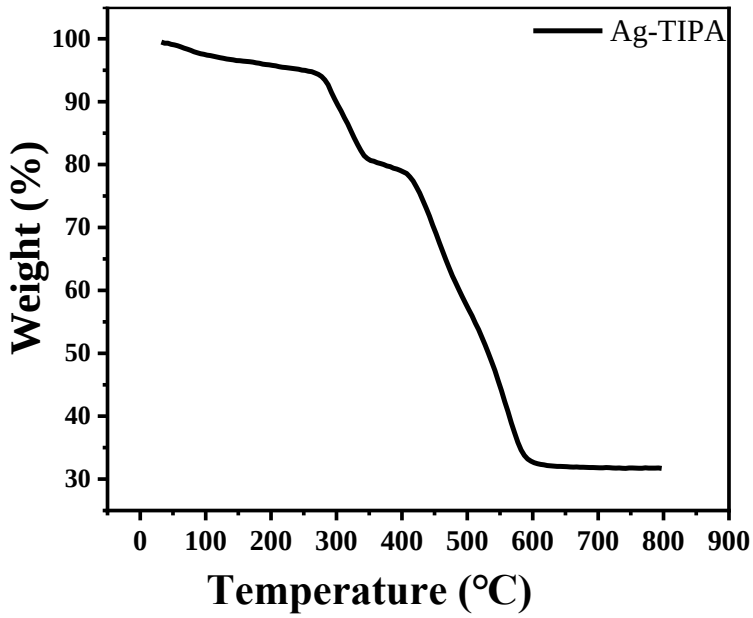

Fig. S3 Thermogravimetric curve of Ag-TIPA.

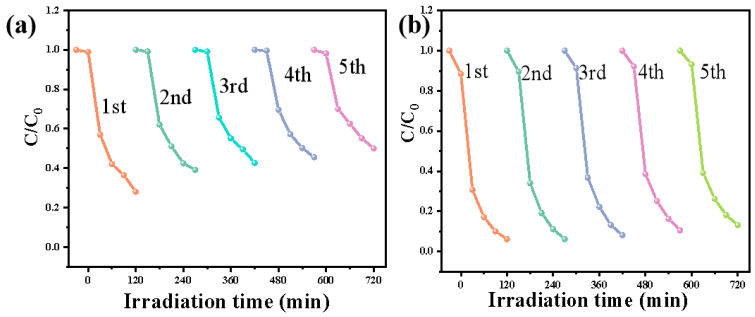

Fig. S4 The photocatalytic degradation of CIP catalyzed by (a) TIPA and (b) Ag-TIPA for five runs.

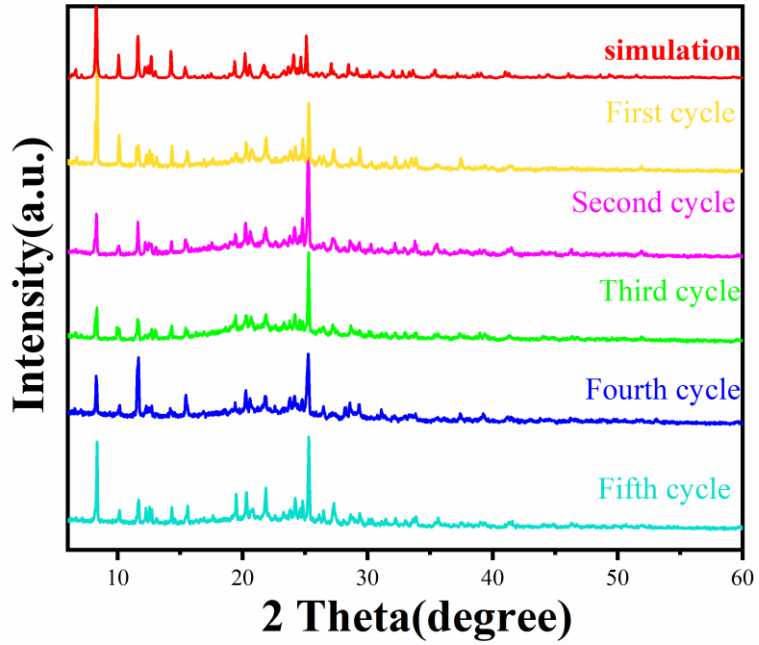

Fig. S5 A comparison of PXRD patterns of Ag-TIPA after every catalytic run for the degradation of CIP.

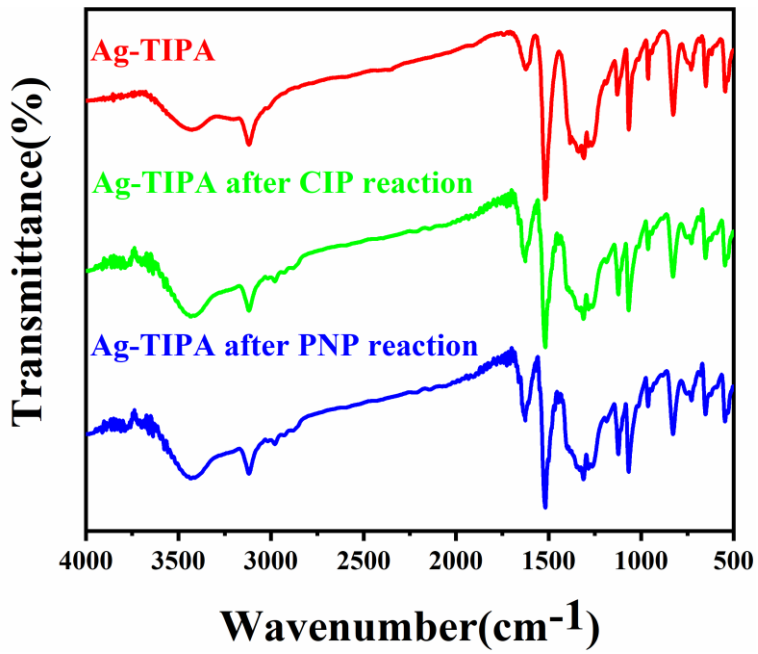

Fig. S6 FT-IR spectra of Ag-TIPA before and after catalysis.

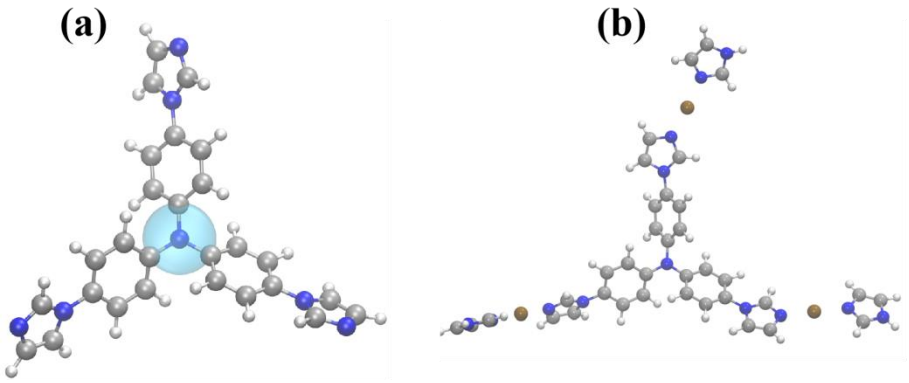

Fig. S7 Electron-hole DFT calculation model for (**a**) TIPA and (**b**) Ag-TIPA.

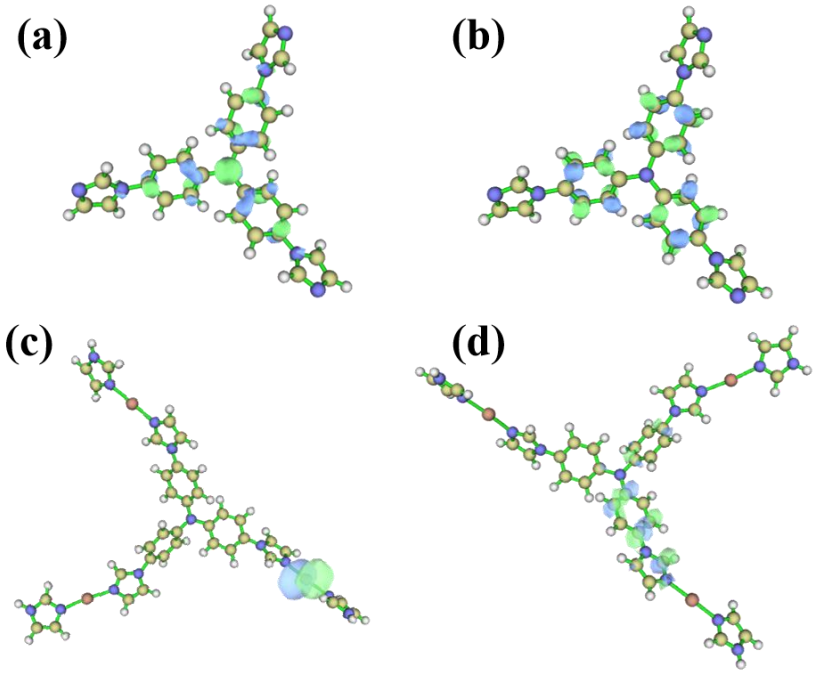

Fig. S8 (**a**) HOMO and (**b**) LUMO of TIPA; (**c**) HOMO and (**d**) LUMO of Ag-TIPA.

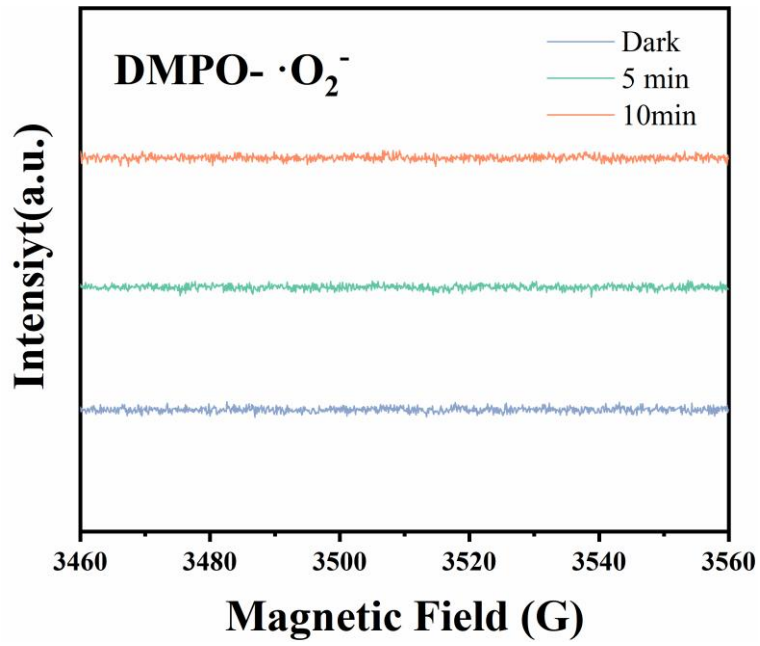

Fig. S9 ESR spectra of Ag-TIPA for DMPO-·O_2^- in the dark and under UV-visible light irradiation.

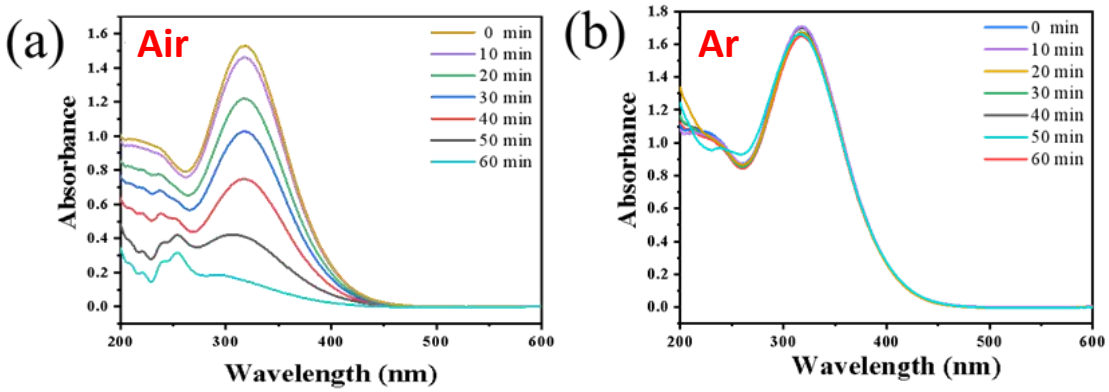

Fig. S10 (**a**) UV/Vis absorption spectrum of Ce(IV) with treatment of Ag-TIPA for H_2O_2 production in air. (**b**) UV/Vis absorption spectrum of Ce(IV) with treatment of Ag-TIPA for H_2O_2 production in argon protection.

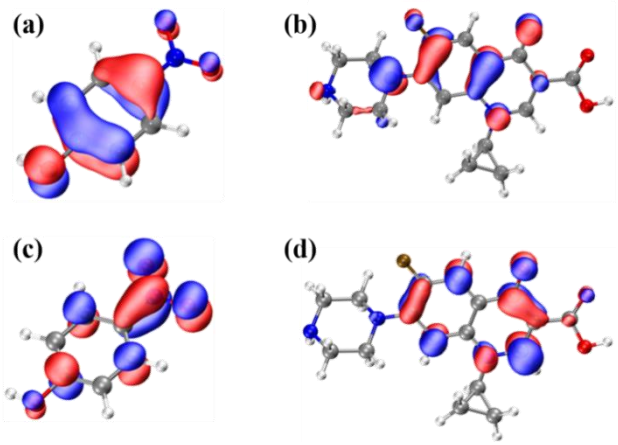

Fig. S11 HOMO of (**a**) PNP and (**b**) CIP; LUMO of (**c**) PNP and (**d**) CIP.

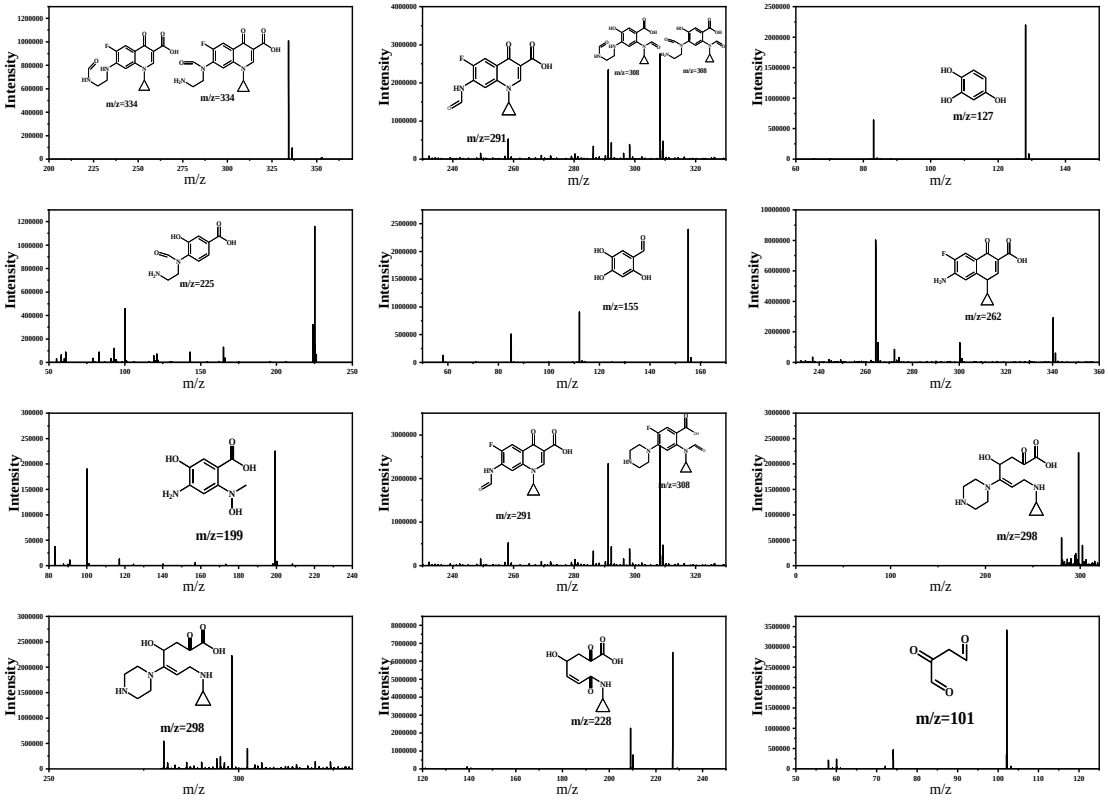

Fig. S12 Mass spectra of intermediates during ciprofloxacin degradation.

Table S1. Crystallographic data for Ag-TIPA.

Coordination polymer	Ag-TIPA
Formula	$C_{162}H_{126}Ag_9N_{51}O_{27}$
Formula weight	4189.96
Temperature	296.15 K
Crystal system	orthorhombic
Space group	*-P 2ab 2bc*
a (Å)	15.2521(9)
b (Å)	27.1930(18)
c (Å)	34.360(2)
α (°)	90
β (°)	90
γ (°)	90
V (Å^3)	14250.8(15)
Z	3
Goof	1.033
R indices [I>2sigma(I)]	R_1 = 0.0671, wR_2 = 0.1762
R indices (all data)	R_1 = 0.1032, wR_2 = 0.2038

Table S2. Bond lengths and bond angles of Ag-TIPA.

Bond lengths	[Å]	Bond angles	[°]
Ag(01)-N51#1	2.101(5)	N51#1-Ag(01)-N11	175.2(2)
Ag(01)-N11	2.104(5)	N12-Ag(02)-N71	178.9(2)
Ag(02)-N12	2.105(6)	N52-Ag(03)-N72#2	175.4(3)
Ag(02)-N71	2.108(5)	C163-N53-Ag(04)	117.0(9)
Ag(03)-N52	2.095(6)	C173-N53-Ag(04)	138.6(9)
Ag(03)-N72#2	2.095(5)	C13-N13-Ag(05)	118.5(13)
Ag(04)-N53	2.258(14)	C23-N13-Ag(05)	132.4(15)
Ag(05)-N13	2.136(18)		

Table S3. ICP-MS analytic data from the solution of Ag-TIPA-catalyzed CIP degradation after fifth cycle.

Number of samples	Ag-TIPA
Sample volume V（mL）	5
Constant volume V_o (mL)	10
Test element	Ag
Test solution element concentration C_o(mg/L)	0.000
Dilution ratio	2
Elemental concentration C_1 in the original solution of digestion solution (mg/L)	0
Elemental content C_x in test sample (mg/L)	0.0

Table S4. A comparison on photodegradation efficiency among the present study and previous reports.

Pollutant (mg/L)	Photocatalyst (g L^{-1})	Light source	Reaction time (min)	Degradation %	Rate constant	Ref.
CIP	Ag-TIPA (1.0)	UV light	120	94	0.023	this work
PNP			75	96	0.043	
P-NP	Graphene/ZnO (1.0)	UV light	180	95	0.016	[1]
P-NP	rGO/ZrO_2/Ag_3PO_4	UV light	90	98.3	0.043	[2]
P-NP	ZnO-NCP (0.25)	UV light	180	60	0.005	[3]
P-NP	Ln-doped ZnO (1.0)	UV light	195	81.63	0.008	[4]
P-NP	ZnO (1.5)	UV light	90	97.7	0.038	[5]
P-NP	Ag-ZnO (2.0)	UV light	180	100	0.039	[6]
P-NP	CuO/ZnO	Sunlight	180	85	0.010	[7]
P-NP	CeO_2 /ZnO (1.5)	UV light	200	95	0.015	[8]
IP	Fe-MOF@BiOBr/ M−CN−50 (0.625)	Xe lamp	120	93	0.022	[9]
CIP	0D/2D WS_2/BiOBr (1.0)	Xe lamp	100	92	0.025	[10]
CIP	BiOAc/BiOBr (0.5)	LED light	120	85	0.022	[11]
CIP	La^{3+}-2D-g-C_3N_4 (1.0)	UVA light	400	93	0.006	[12]

Table S5. Electron and hole analysis index for TIPA and Ag-TIPA.

S0-S1	**D(Å)**	**T (Å)**	**H (Å)**	**Δσ (Å)**	**Sm (a.u.)**	**Sr (a.u.)**	**HDI**	**EDI**
TPA	0.014	-0.981	3.428	-0.001	0.3688	0.6357	9.32	5.60
Ag-TPA	4.406	2.034	3.746	1.526	0.17643	0.38815	4.60	5.52
S0-S2	**D (Å)**	**T (Å)**	**H (Å)**	**Δσ (Å)**	**Sm (a.u.)**	**Sr (a.u.)**	**HDI**	**EDI**
TPA	1.476	-1.071	3.622	0.294	0.3918	0.6592	9.46	6.37
Ag-TPA	2.091	-0.980	4.120	0.690	0.31878	0.61195	4.31	4.38
S0-S3	**D (Å)**	**T (Å)**	**H (Å)**	**Δσ (Å)**	**Sm (a.u.)**	**Sr (a.u.)**	**HDI**	**EDI**
TPA	1.470	-0.928	3.621	0.293	0.4031	0.6681	9.46	6.37
Ag-TPA	2.657	-0.198	3.689	1.829	0.27439	0.54673	4.46	4.28

Table S6. Fukui Index and Orbital weight double descriptor values for PNP.

Atom index	OW f^+	OW f^-	OW fo	OW DD
C1	0.04438	0.11452	0.07945	-0.07014
C2	0.08042	0.10361	0.09201	-0.02319
C3	0.04454	0.10775	0.07615	-0.06321
C4	0.08808	0.07495	0.08151	0.01313
C5	0.07022	0.13304	0.10163	-0.06281
C6	0.08306	0.17180	0.07743	0.01126
H7	0.00391	0.00835	0.00613	-0.00444
H8	0.00399	0.00783	0.00591	-0.00384
H9	0.00981	0.00572	0.00776	0.00409
H10	0.00917	0.00541	0.00729	0.00377
N11	0.19964	0.03128	0.11546	0.16835
O12	0.16794	0.10967	0.13881	0.05827
O13	0.16680	0.11025	0.13853	0.05655
O14	0.02567	0.10922	0.06744	-0.08354
H15	0.00228	0.00653	0.00440	-0.00426

Table S7. Fukui Index and Orbital weight double descriptor values for CIP.

Atom index	OW f^+	OW f^-	OW fo	OW DD
C1	0.05686	0. 03558	0.04622	0. 02128
N2	0.05118	0. 04909	0.05014	0. 00209
C3	0. 14014	0. 02074	0. 08044	0. 11940
C4	0. 06968	0. 06159	0. 06564	0. 00809
C5	0.07994	0.03247	0. 05620	0. 04747
C6	0.06612	0. 06364	0. 06488	0. 00249
O7	0.01132	0. 01042	0. 01087	0. 00089
C8	0.05024	0. 01298	0. 03161	0. 03726
C9	0.07485	0. 03043	0. 05264	0. 04443
C10	0.05436	0. 05144	0. 05290	0. 00292
C11	0.07536	0. 03759	0. 05647	0. 03778
C12	0.06322	0. 04598	0. 05460	0.01724
N13	0.01881	0. 10036	0. 05958	-0. 08155
C14	0. 00327	0. 02101	0.01214	-0. 01774
C15	0.00639	0. 02273	0. 01456	-0. 01634
C16	0 00095	0. 01456	0. 00776	-0. 01361
N17	0. 00047	0. 09058	0. 04552	-0. 09010
C18	0.00111	0. 01537	0. 00824	-0. 01426
F19	0.00874	0. 01737	0. 01306	-0. 00863
C20	0.00798	0. 00633	0. 00715	0. 00165
O21	0.06412	0. 15154	0. 10783	-0. 08742
O22	0. 03965	0. 04557	0. 04261	-0. 00592
C23	0.00314	0. 00442	0. 00378	-0. 00129
C24	0.00303	0. 00199	0. 00251	0. 00104
H25	0.01529	0. 00201	0. 00865	0. 01328
H26	0.00098	0. 00110	0.00104	-0. 00013
H27	0.00789	0. 00325	0. 00557	0. 00463
H28	0.0067	0.0039	0.0053	0. 00280
H29	0.00133	0. 00273	0. 00203	-0. 00140
H30	0.00154	0. 00892	0.00523	-0. 00738
H31	0. 00235	0.00953	0.00594	-0. 00717
H32	0 00108	0.00284	0. 00196	-0. 00176
H33	0.00027	0. 00181	0.00104	-0. 00154
H34	0.00025	0. 00310	0. 00168	-0. 00285
H35	0.00047	0.00692	0. 00370	-0. 00645
H36	0. 00053	0.00206	0. 00129	-0. 00152
H37	0.00031	0. 00311	0. 00171	-0. 00280
H38	0. 00422	0.00338	0. 00380	0. 00084
H39	0.00129	0. 00042	0. 00085	0. 00087
H40	0.00148	0. 00064	0. 00106	0. 00084
H41	0.00078	0. 00021	0.00049	0. 00057
H42	0.00239	0. 00034	0. 00136	0.00205

Table S8. Target ion information table of CIP.

intermediate species	structural formula	appearance time	relative molecular mass M	anion [M+H]
$C_{16}H_{16}FN_3O_4$	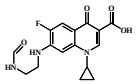	11.32	333	334
$C_{16}H_{16}FN_3O_4$	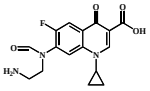	11.32	333	334
$C_{14}H_{17}FN_3O_5$	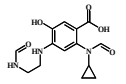	13.53	307	308
$C_{14}H_{17}FN_3O_5$	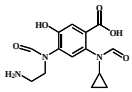	13.53	307	308
$C_{10}H_{12}N_2O_4$	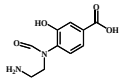	11.32	224	225
$C_7H_6O_4$	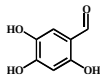	10.01	154	155
$C_6H_6O_3$	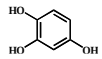	12.25	126	127
$C_{14}H_{12}FNO_3$	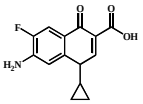	10.01	261	262
$C_8H_{10}N_2O_4$	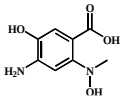	10.91	198	199
$C_{15}H_{18}FN_3O_3$	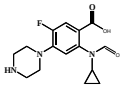	13.53	307	308
$C_{14}H_{23}N_3O_4$	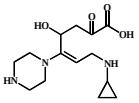	9.19	297	298
$C_{10}H_{13}NO_5$	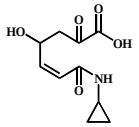	1.43	227	228
$C_4H_4O_3$		15.91	100	101

Table S9. Target ion information table of PNP.

intermediate species	structural formula	appearance time	relative molecular mass M	anion [M+H]
p-nitrophenol	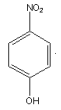	1.68	139.03	138.02
maleic acid	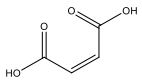	1.69	116.01	115.00
oxalic acid	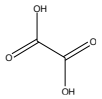	1.9	90.00	89.02
nitrobenzene		1.87	123.03	122.02
dinitrophenol		2.15	184.01	183.00
pyruvic acid	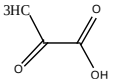	2.01	88.02	87.00
hydroquinone	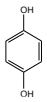	3.4	154.02	154.01
p-pyrocatechol	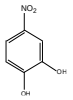	4.92	110.00	109.01
nitric acid		1.80	63	61.99
acetic acid	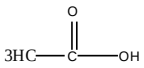	1.96	60.05	59.01

References

1. D. Kale, P. Thakur, *J. Porous Mater.,* 2015, **22**, 797-806.
2. H. Anwer, J.-W. Park, *J. Hazard. Mater*., 2018, **358**, 416-426.
3. A. Nezamzadeh-Ejhieh, S. Khorsandi, *J. Ind. Eng. Chem*., 2014, **20**, 937-946.
4. M. Khatamian, A. A. Khandar, B. Divband, M. Haghighi, S. Ebrahimiasl, *J. Mol. Catal. A Chem*., 2012, **365**, 120-127.
5. D. Rajamanickam, M. Shanthi, *Arab. J. Chem*., 2016, **9**, S1858-S1868.
6. B. Divband, M. Khatamian, G. R. K. Eslamian, M. Darbandi, *Appl. Surf. Sci*., 2013, **284**, 80-86.
7. M. T. Qamar, M. Aslam, I. M. I. Ismail, N. Salah, A. Hameed, *ACS Appl. Mater. Interfaces,* 2015, **7**, 8757-8769.
8. K. Negi, M. Kumar, M. S. Chauhan, *Mater. Chem. Phys*., 2019, **226**, 59-65.
9. Y. Pan, X. Hu, D. Shen, Z. Li, R. Chen, Y. Li, J. Lu, M. Bao, *Sep. Purif. Technol*., 2022, **295**, 121216.
10. S. Fu, W. Yuan, X. Liu, Y. Yan, H. Liu, L. Li, F. Zhao, J. Zhou, *J. Colloid Interface Sci.,* 2020, **569**, 150-163.
11. H. Liu, B. Wang, M. Chen, H. Zhang, J. Peng, L. Ding, W. Wang, *Sep. Purif. Technol*., 2021, **261**, 118286.
12. S. K. Kuila, D. K. Gorai, B. Gupta, A. K. Gupta, C. S. Tiwary, T. K. Kundu, *Chemosphere,* 2021, **268**, 128780.